Pure Appl. Geophys.

https://doi.org/10.1007/s00024-020-02554-5

Pure and Applied Geophysics

Analysis of Time Dynamical Features in Intraplate Versus Interplate Seismicity: The Case Study of Iquique Area (Chile)

Luciano Telesca,[1] Denisse Pastén,[2] and Víctor Muñoz[2]

Abstract—The intraplate and interplate seismic catalogues of Iquique (Chile) area were investigated by using seismological (*b* value of the Gutenberg–Richter law), fractal (Allan Factor and detrended fluctuation analysis) and topological (Horizontal Visibility Graph) methods. The two catalogues show different stress state indicated by the different *b* value, larger for the intraplate seismicity. The interplate seismicity shows significant time-clustering behavior of the earthquake occurrence times at large time scales, while the time distribution of the intraplate earthquakes seems to be featured by random fluctuations without any significant sign of time-clustering. Different role seems to be played by aftershocks in the two investigated seismic zones, revealed by the different time distribution of the aftershock-depleted catalogue of the intraplate zone, which remains Poissonian for most of the time scales, and the interplate zone that still keeps its clustering phenomenon but at higher timescales, thus shortening its clustering time scale range. Furthermore, the interevent times of the interplate catalogue are characterized by persistent dynamics even after removing the aftershocks, while uncorrelated fluctuations characterize the behavior of interevent intervals of the whole as well as aftershock-depleted intraplate catalogue. Additionally, the magnitudes of both catalogues are characterized by time-reversibility before and after the aftershock removal; while the interevent times of intraplate catalogue change their status from time-irreversibility to time-reversibility after removing the aftershocks. The obtained results seem to evidence a different role played by the aftershocks in the intraplate and interplate zones, that needs to be further explored.

Keywords: Interplate seismicity, intraplate seismicity, earthquake, time series analysis.

1. Introduction

The northern zone of Chile was struck by four major seismic events in the past centuries: in 1543, 1615, 1768 and 1877 (Ruiz and Madariaga 2018). The magnitude proposed for the last megathrust occurred in 1877 in the central Andes subduction zone is M_w= 8.7 (Comte and Pardo 1991) and affected Pisagua and Iquique (Vidal Gormaz 1877; Montessus de Ballore 1911–1916). It has still been debating if all these major events were interplate or intraplate intermediate depth (Ruiz and Madariaga 2018). On the other hand, after the 1877 megathrust (that also triggered a large tsunami), earthquakes with magnitudes greater than M_w 7.0 occurred in the northern zone of Chile, such as Tocopilla earthquake in 1967 (M_w 7.4) and 2007 (M_w 7.8), Tarapacá earthquake in 2005 (M_w 7.8) and Antofagasta earthquake in 1995 (M_w 8.0) (Malgrange and Madariaga 1983; Ruegg et al. 1996; Peyrat et al. 2010); among these only the Tarapacá earthquake is intraplate intermediate depth, while the others are deep plate interface (Ruiz and Madariaga 2018). The seismic activity in this region has been studied during years (Kausel 1986; Comte and Pardo 1991; Lomnitz 2004; Métois et al. 2012). This region is not homogeneous and shows a distribution of the average seismic coupling, separated in segments and intersegments, which could produce a megathrust with magnitude greater than M_w= 8.0 (Métois et al. 2012). In particular, the region between Arica and Iquique is characterized by a low value of the coupling between the Nazca and South American plates, but is able to generate subduction earthquakes with magnitudes between M_w= 6.0 and M_w= 7.0, possibly produced by the bathymetry of the inferior slab. On the other hand, this region has had an unusual intraplate activity, with earthquakes that could reach the magnitude of M_w= 7.7

[1] Institute of Methodologies for Environmental Analysis, National Research Council, 85050 Tito, PZ, Italy.

[2] Departamento de Física, Facultad de Ciencias, Universidad de Chile, Santiago, Chile. E-mail: denisse.pasten.g@gmail.com

Published online: 24 July 2020

Deformation has accumulated in this zone for more than 140 years, and the Iquique 2014 M_w= 8.2 earthquake was identified, in principle, as the megathrust expected for the North of Chile. However, this large earthquake generated a rupture of 250 km, less than expected in this region. However, a larger earthquake is still expected in the north as well as in the south of the rupture zone of the Iquique 2014 earthquake.

In a recent study a marked difference was found in the seismic moment (M_0), the corner frequency (f_c) and the energy radiated (E_R), between shallow depth and intermediate-depth earthquakes in the northern zone of Chile (Derode and Campos 2019), showing the relevance to analyze the seismicity of this region considering the intraplate and interplate seismic events.

In this study, we aim at characterizing the interplate and intraplate seismicity of the seismic area where the M_w= 8.2 Iquique earthquake 2014 occurred by using complexity approaches that could be helpful to better understand the seismic process occurring in the far north of Chile.

We jointly employed several measures (seismological, fractal and topological) to deeply characterize the time dynamics of the seismicity of this particular area of Chile: the b value of the Gutenberg-Richter law, the Allan factor, the Detrended Fluctuation Analysis (DFA) and the Horizontal Visibility Graph (HVG). The different statistical techniques used to investigate this area are able to highlight different dynamical features of the interplate and intraplate seismicity and to furnish a more exhaustive picture of the seismic process.

2. Tectonic and Seismic Setting

The Chilean coast has a long subduction zone between the Nazca Plate and the South American plate. This boundary has a high velocity of convergence which is about 6–7 cm year^{-1}. Particularly, the North of Chile has shown an important seismic gap from the last large earthquake in 1877 (M_w = 8.8), which means that this region presents a high seismic hazard, including a high tsunami hazard. Since this last large earthquake, some significant seismic events have occurred in this zone, the 1967 M_w = 7.4, on the north Mejillones Peninsula; the 1995 M_w = 8.1 Antofagasta earthquake in the south of the Mejillones Peninsula; the 2007 M_w = 7.7 Tocopilla earthquake and the 2005 M_w = 7.7 Tarapacá deep intraslab event, in the inner zone of this region. These events have shown that this is an active seismic area with enough strain accumulated to host an earthquake greater than M_w = 8.8. In the latest 20 years two seismic events have ruptured within this long seismic gap that is located from the southern coast of Peru until the northern coast of Chile: the 2001 M_w = 8.4 Arequipa earthquake and the 2014 M_w = 8.2 Iquique earthquake have filled this long gap partially. We have concentrated in the study of the M_w = 8.2 Iquique earthquake. This zone was studied previously by Métois et al. (2016) and they concluded that this region is an intersegment zone, in the long seismic gap, with an average coupling lower than the mean value of coupling for the gap. This megathrust had a particular behavior because the seismic activity increased significantly 3 weeks before the M_w = 8.2 large earthquake with more than 80 seismic events greater than M_w = 4.0, and had a great activity after the main event, activity which included an aftershock of M_w = 7.7, occurred in the south of the rupture zone, with more than 140 aftershocks greater than M_w= 4.0 (Hayes et al. 2014).

In this study, we used the earthquake catalogue compiled by the Integrated Plate boundary Observatory Chile (IPOC) (Sippl et al. 2018a, b), comprising the area between 19.0° S and 23.5° S Latitude and between 69.0° W and 71.5° W Longitude, with depth less than 250 km, and from January 01, 2007 until December 31, 2014. In particular we analysed the interplate and intraplate earthquakes, indicated as P1 and P3 data in Sippl et al. (2018a).

3. Methods and Data Analysis

3.1. The b Value of the Gutenberg–Richter Law

The Gutenberg–Richter (GR) law states that the cumulative number N of earthquakes with magnitude larger than a threshold M_{th}, behaves as a power-law expressed by $N = 10^{a-bMth}$, where a represents the

earthquake productivity, and b is a critical parameter indicating the proportion of small events respect to the large ones (Gutenberg and Richter 1944; Ishimoto and Iida 1939). The larger the b value, the larger the proportion of small events respect to the large earthquakes. The b value can be considered as an indirect measure of the stress crustal conditions (Scholz 1968; Wyss 1973). Its numerical value can also indicate if purely tectonic earthquakes ($b < 1.5$–1) or volcano-tectonic earthquakes ($b > 1.5$), which is mainly due to hydraulic fracturing of the host rock induced by over pressurized magma and/or associated fluids, are taking place. The b value was also found in the distribution of acoustic emissions events, generated in laboratory-created fault zones (Goebel et al. 2013). Temporal and spatial variations of the b-value were analysed to get information about the tectonic regime (Tormann et al. 2015). The negative correlation between b value and differential stress (Spada et al. 2013), confirmed that the b could be considered as an indirect stress meter in the Earth's crust (Schorlemmer et al. 2005). The reliable estimation of the b value, then, is important to discriminate different evolution stages of seismicity with clear implications in the seismic hazard assessment (Naylor et al. 2009).

The b value can be calculated by the least square linear regression method on the logarithm of the cumulative number of earthquakes (Kárník and Klíma 1993). The least square linear regression method is a curve fitting technique that minimizes the summed squares of the residuals. Applying this procedure the estimation of the b value is the following:

$$b = \frac{N\sum_{i=1}^{N} M_{th,i}\log_{10} N_{M\geq M_{th,i}} - \sum_{i=1}^{N} M_{th,i}\sum_{i=1}^{N}\log_{10} N_{M\geq M_{th,i}}}{N\sum_{i=1}^{N}\left(M_{th,i}\right)^2 - \left(\sum_{i=1}^{N} M_{th,i}\right)^2}. \quad (1)$$

Its error is given by the following formula

$$\sigma_b = \frac{1}{\sqrt{N-2}}\sqrt{\frac{\sum_{i=1}^{N}\left(\log_{10} N_{M\geq M_{th,i}} - \log_{10}\hat{N}_{M\geq M_{th,i}}\right)^2}{\sum_{i=1}^{N}\left(M_{th,i} - <M>\right)^2}} \quad (2)$$

where $\log_{10}\hat{N}_{M\geq M_{th,i}}$ represents the linear regression estimate of $\log_{10} N_{M\geq M_{th,i}}$.

As alternative to the estimation of b value by the least square linear regression method, there is the estimation by the maximum likelihood:

$$b = \frac{\log_{10}(e)}{\langle M\rangle - \left(M_c - \Delta M_{bin}/2\right)}, \quad (3)$$

where $\langle M\rangle$ is the mean magnitude of the sub-set of seismic events with magnitude larger or equal to the completeness magnitude M_c and ΔM_{bin} represents the binning width of the catalogue (Aki 1965; Utsu 1999). Its error is calculated by using the Shi and Bolt's formula (1982):

$$\sigma_b = 2.3b^2\sqrt{\frac{\sum_{i=1}^{N}\left(M_i - \langle M\rangle\right)^2}{N(N-1)}}. \quad (4)$$

3.2. Magnitude of Completeness

Several methods have been proposed to perform the estimation of the completeness magnitude. Wiemer and Wyss (2000) proposed the method of the maximum curvature (MAXC): M_c is the magnitude that corresponds to the highest frequency of earthquakes in the binned frequency-magnitude distribution. The entire-magnitude-range (EMR) (Woessner and Wiemer 2005) is another method that considers the whole magnitude set, subdivided in a complete and incomplete part. The complete part is modeled by a power-law with a- and b-value estimated by the Aki–Utsu's formula; the incomplete part is modeled by a normal cumulative distribution function that describes the detection capability. The incomplete part is, thus, a function of magnitude that is fitted to the data, and depends on μ (magnitude at which 50% of the seismic events are detected), σ (the standard deviation describing the width of the range where earthquakes are partially detected) and M_c, which represents the lower limit of magnitudes that are detected with probability 1; the completeness magnitude M_c is that value maximizing the log-likelihood function of a, b, μ and σ. A third method was proposed by Wiemer and Wyss (2000) and was based on the goodness-of-fit (GFT) given by the absolute difference of the number of earthquakes in the magnitude bins between the observed cumulative frequency-magnitude distribution and the synthetic

ones calculated with the a- and b-values of the observed dataset for $M \geq M_{th}$; the GFT is, thus, a function of M_{th} that is the M_c when the 90% of the observed data are well modeled by a straight line. All these methods are implemented in the freely available software package ZMAP (Wiemer 2001). Generally, all these methods could give different values of the completeness magnitude, this making more reasonable to estimate the b value by the Kijko and Smit's approach rather than by applying the Aki–Utsu's formula.

3.3. Aftershock Depletion by Using the Nearest-Neighbour Algorithm

Among the several techniques that exist to remove aftershocks from a seismic sequence, we used the declustering technique based on nearest-neighbour (NN) distance of events in space–time-energy domain (Zaliapin et al. 2008).

If the earthquake i is characterized by occurrence time t_i, epicenter (lat_i, lon_i) and magnitude m_i, we aim to identify for each earthquake j its possible parent, which is an earlier earthquake i that is the closest, in some sense, to j among all earlier earthquakes. Following Baiesi and Paczuski (2004), the distance between earthquakes i and j is defined as:

$$n_{ij} = \begin{cases} c\tau_{ij} r_{ij}^{d_f} 10^{-bm_i} & \tau_{ij} > 0 \\ \infty & \tau_{ij} \leq 0 \end{cases} \qquad (5)$$

where τ_{ij} is the time interval (in years) between events i and j (positive if earthquake i occurred before earthquake j, negative if viceversa) r_{ij} their spatial distance (in km), d_f is the fractal dimension of the spatial distribution of the epicenters, and b the parameter of the Gutenberg–Richter law (Zaliapin and Ben-Zion 2016).

The distance n_{ij} can be conveniently factorized as $n_{ij} = T_{ij}R_{ij}$, where

$$\begin{cases} T_{ij} = \tau_{ij} 10^{-qbm_i} \\ R_{ij} = r_{ij}^{d_f} 10^{-(1-q)bm_i} \end{cases} \qquad (6)$$

The choice of $q = 0.5$ assigns equal weight to space and time components (Peresan and Gentili, 2020). Zaliapin et al. (2008) demonstrated that the 1D empirical distribution of the NN distances and the 2D density map of its components (R, T), obtained from models of Poissonian seismicity and individual clusters, are both unimodal; while the distributions that are obtained from real seismicity and from models of clustered seismicity are rather bimodal. Such bimodality is used to discriminate the background seismicity from clusters (Zaliapin and Ben-Zion 2013) that are those earthquakes whose NN distance is less than a specified threshold n_0. The threshold n_0 can be selected as the maximum likelihood boundary between the two modes of a 2-component 1-D Gaussian mixture model. The NN algorithm is, then, a robust, data-driven tool to uniformly identify clusters associated with main shocks from a wide magnitude range, and just requires three parameters as input, the Gutenberg–Richter b-value, the fractal dimension of epicentres d_f, and the threshold distance n_0.

3.4. The Allan Factor

The Allan Factor (AF) is a measure for discriminating between time-clusterized earthquake sequences or not. Differently from the coefficient of variation, the AF gives also information on which timescales are involved in the time-clustering behavior of the sequence. Dividing the time axis into contiguous counting windows of same duration τ (which is the timescale), we can construct a series of counts $\{N_k(\tau)\}$, counting how many earthquakes fall in the k-th window (Thurner et al. 1997). The AF, then, is defined as

$$AF(\tau) = \frac{\left\langle (N_{k+1}(\tau) - N_k(\tau))^2 \right\rangle}{2\langle N_k(\tau) \rangle}, \qquad (7)$$

and it is related to the variability of successive counts (Thurner et al. 1997); the symbol $\langle \ldots \rangle$ indicates the average value. The AF has been largely used to investigate the time dynamics of point processes of different types (Telesca et al. 2000, 2001; Telesca and Lovallo 2008).

If the earthquake process is Poissonian, the AF slightly fluctuates around 1 at all timescales [except for very large timescales, due to finite-size effects (Telesca et al. 2012)]; but if the earthquake process is clusterized the AF changes with the timescale τ. In

particular, if the earthquake process is fractal (self-similar) in time, the AF behaves as a power-law (scaling behavior):

$$AF(t) = 1 + \left(\frac{t}{t_1}\right)^{\alpha}, \tag{8}$$

where the exponent α quantifies the strength of clusterization; τ_1 is the so-called fractal onset time and marks the lower limit for significant scaling behavior in the AF (Thurner et al. 1997). Therefore, if $\alpha \sim 0$ the earthquake process is Poissonian, while if $\alpha > 0$ it is clusterized.

3.5. The Detrended Fluctuation Analysis of Interevent and Magnitude Time Series

Since the Detrended Fluctuation Analysis (DFA) has been proposed to identify long-range correlations in non-stationary series (Peng et al. 1995), several natural processes have been investigated by means of this technique (Telesca and Lovallo 2009, 2010, 2011; Telesca et al. 2012).

In particular, the application of the DFA to earthquake magnitudes was performed by Telesca et al. (2016), who found that the DFA scaling exponent increased during the reactivation periods of the volcanic activity at El Hierro, Canary Islands (Spain) in the 2011–2014. Varotsos et al. (2014) interpreted the results of DFA of earthquake magnitudes in terms of earthquake prediction. Lennartz et al. (2008) analyzed the long-range correlations of the magnitude series of earthquakes occurred in Northern and Southern California by the DFA. Varotsos et al. (2012) found that in California seismicity, the DFA scaling exponent of magnitudes is able to reveal breaks of the long-range correlations before the occurrence of large shocks.

The scaling properties of the seismic interevent time series were investigated by using the DFA in several cases (Telesca and Chen 2019; Telesca et al. 2012).

Analyzing the long-range correlations in earthquake magnitude series and interevent times, thus, is an important step to gain insight into the dynamics of a seismic process.

The DFA method is described below:

(i) the seismic series x_i, where $i = 1,\ldots,N$, and N is the total number of events is integrated and the integrated series y_k is divided into windows of same length n;

(ii) for each n-size window, the least square line $y_{n,k}$ fits y_k and is subtracted from y_k;

(iii) the fluctuation, F_n, is calculated

$$F_n = \sqrt{\frac{1}{N}\sum_{k=1}^{N}\left[y_k - y_{n,k}\right]^2}; \tag{9}$$

(iv) the steps (i)–(iii) are repeated for all the available window sizes n; if the relationship between $F_n \sim n$ is a power-law, the series is long-range correlated:

$$F_n \sim n^{\alpha}; \tag{10}$$

(v) the numerical value of the scaling exponent α informs about which type of temporal correlations the seismic series is characterized of: the series is uncorrelated, if $\alpha = 0.5$; they are persistently correlated (meaning that if the series increases (or decreases) in a period, it tends to increase (or decrease) in the next period), if $\alpha > 0.5$; it is antipersistently correlated (meaning that if the series increases (or decreases) in a period, it tends to decrease (or increase) in the next period), if $\alpha < 0.5$.

3.6. The Horizontal Visibility Graph (HVG)

The visibility graph (VG) method was firstly introduced by Lacasa et al. (2008) as a way to convert time series into graphs, according to some specific geometric rules (Luque et al. 2009; Lacasa et al. 2008); therefore, properties of time series can be put in relationship with the properties of such graphs (Lacasa et al. 2009).

The horizontal visibility graph (HVG) (Luque et al. 2009), is a particular type of visibility graph defined as follows. If $\{x_t\}$ for $t = 1,\ldots,N$ a real-valued time series of N data that act as nodes of the graph. Two nodes i and j in the graph are connected if a horizontal line can join x_i and x_j without interruption by any other intermediate value. The geometric rule of the HVG is:

$$x_i, x_j > x_n, \forall n | i < n < j. \quad (11)$$

The number of the links of a node with any other node of the graph represents its connectivity degree. The connectivity degree distribution can be analysed to derive several properties of the time series, among which, the property of reversibility/irreversibility of a time series. A statistically time reversible stationary process $X(t)$ is defined by the following property: for any N the series $\{X(t_1),\ldots, X(t_N)\}$ and $\{X(t_N),\ldots, X(t_1)\}$ have the same joint probability distribution (Weiss 1975). Gaussian linear processes are time-reversible; while time series irreversibility is a fingerprint of nonlinear dynamics (Kawai et al. 2007; Parrondo et al. 2009). Recently, the idea of irreversibility in time series was linked to that of entropy produced by the physical mechanism generating the series (Roldan and Parrondo 2010). Since from the formal definition of reversibility/irreversibility in time series does not permit the implementation of an optimal algorithm for its quantification (Lacasa et al. 2012), several different techniques have been developed to measure the degree of irreversibility in time series (Yang et al. 2003; Costa et al. 2008 ; Daw et al. 2000; Diks et al. 1995; Gaspard 2004; Cammarota and Rogora 2007; Andrieux et al. 2007; Wang et al. 2005). The majority of these techniques are based on series symbolization: the data range is empirically partitioned (Daw et al. 2000), operation that does not change the reversibility of the transformed series, and the symbol strings occurrences are statistically compared in the forward and backwards series or using compression algorithms (Cover and Thomas 2006). However, the transformed series depend on the range partitioning or the size of the symbol alphabet; and, moreover, possible multiple scales present in the series could be concealed by such a local coarse-graining transformation (Costa et al. 2008). In a recent paper, Lacasa et al. (2012) assessed the irreversibility of a time series on the base of HVG method (Luque et al. 2009; Lacasa et al. 2008, 2009). Using the Kullback–Leibler divergence (Cover and Thomas 2006) between the forward and backward connectivity degree distributions, they proposed a measure of quantification of irreversibility in stationary stochastic time series. Schleussner et al. (2015) used the visibility graph approach to identify signatures of irreversibility in two ocean sediment August sea-surface temperature records from the Norwegian Sea and the central subpolar.

More in detail, splitting the connectivity degree $k(t)$ of the node t in in-going degree $k_{in}(t)$ (the number of links of node t with other past nodes) and out-going degree $k_{out}(t)$ (the number of links with future nodes), such that $k(t)= k_{in}(t)+ k_{out}(t)$, we can define the $P_{in}(k)= P(k_{in}= k)$ and the $P_{out}(k)= P(k_{out}= k)$ as the in-going and out-going degree distributions.

The Kullback–Leibler divergence (KLD) (Cover and Thomas 2006) can be used to measure the distributional distance between $P_{out}(k)$ and $P_{in}(k)$:

$$D(P_{in}//P_{out}) = \sum_{x\in X} P_{in}(x)\log\frac{P_{in}(x)}{P_{out}(x)} \quad (12)$$

This measure is always positive except when both probability distributions are equal $P_{out}= P_{in}$. The KLD is statistically significant, as it is proved by the Chernoff–Stein lemma. The KLD is a measure of "distinguishability", therefore the higher the distinguishability between P_{out} and P_{in}, the larger the $D(P_{in}||P_{out})$.

4. Results

We analysed the seismicity of intraplate and interplate seismicity with local magnitude larger or equal to 1.4 of Iquique area (Chile) from January 2007 to December 2014. Figure 1 shows the spatial distribution of the seismicity studied, and Fig. 2 shows a cross section where the profile of the subduction zone is clear. Figure 3 shows the non-cumulative (NCFMD) and cumulative (CFMD) frequency-magnitude distribution of the intraplate and interplate seismicity of Iquique area.

The completeness magnitude M_c was calculated by using the methods described in Sect. 3.2. The completeness magnitude for the interplate seismic catalogue is 2.2 (MAXC), 2.1 (GFT at 90%) and 2.5 (EMR), while for the intraplate seismic catalogue is 2.1 (MAXC), 2.0 (GFT at 90%) and 2.2 (EMR).To be conservative, we chose the completeness magnitude as the largest among the three ones, namely that one calculated by EMR method, thus 2.5 for the interplate

and 2.2 for the intraplate seismicity. Thus, all the following analyses were performed on the earthquakes with magnitude larger or equal to 2.2 for the intraplate catalogue ($N = 2015$) and 2.5 for the interplate catalogue ($N = 5780$). The Gutenberg–Richter b value was calculated by the least square linear regression method (LSR) and the Aki–Utsu's formula (A–U). Table 1 shows synoptically the b value calculated by using the two mentioned methods. Figure 4 shows the CFMD of each seismic catalogue (starting from the completeness magnitude) and the G-R law obtained for each b value.

Different values of b are obtained by using the two methods; the b value obtained by using the A–U method is smaller than that obtained by the LSR method. The b value estimated by the A–U method depends on the completeness magnitude and is more sensitive to the amount of smaller events than larger

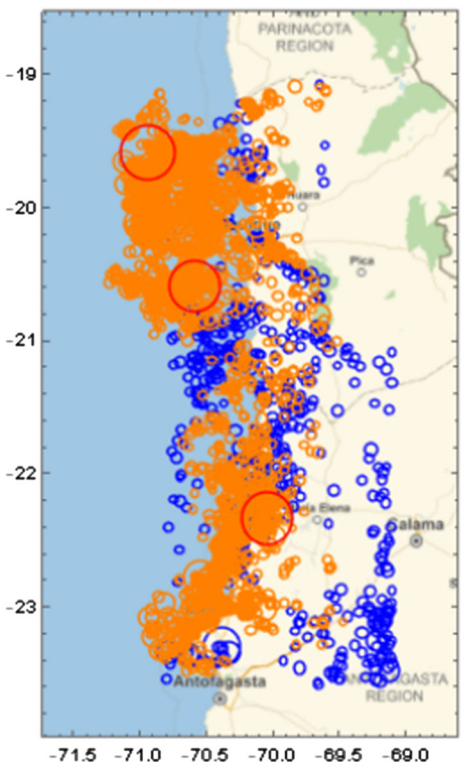

Figure 1
Map of the epicenter location for the region studied in the far north of Chile. The size of circles (blue for intraplate and orange for interplate) is proportional to the magnitude. The seismic events shown in this map are greater than M_w= 4.0. Red circles are seismic events with magnitudes greater than M_w= 7.0

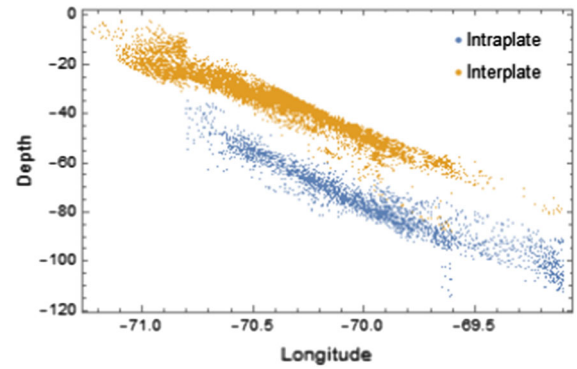

Figure 2
Transverse cut map of the hypocentre locations for the region studied

(Han et al. 2015). The b value calculated by the LSR method is very sensitive to large events (that play the role of outliers in the seismic sequence) (Han et al. 2015). The two methods seem to give consistent values of b for both the catalogues. However, it is clear that the interplate seismicity is characterized by a b-value lower than that of the intraplate seismicity. The interplate catalogue contains the largest event occurred at Iquique ($M = 8.1$). Considering that the stress in the interplate and intraplate are expected to be different, the difference in their respective b values could be consistent with previous results (Scholz 2015), if the lower b values for the interplate catalogues can be related to larger stress in that zone.

We declustered both the catalogues by means of the NN algorithm (Zaliapin et al. 2008). We depleted the catalogues limited to data completeness (Peresan and Gentili 2020), thus the minimum magnitude of the catalogues are 2.5 for the interplate and 2.2 for the intraplate catalogue. Since the fractal dimension of the spatial epicentral distribution is one of the input parameters to the NN algorithm, we firstly calculated the fractal dimension of spatial distribution of both seismicity, by using the Grassberg–Procaccia method (Grassberger and Procaccia 1983), which is well known in spatial statistics for its efficiency and low noisiness in estimating the correlation dimension (that is the fractal dimension) of datasets with even small size (Doxas et al. 2010). If $N_{R<r}$ is the number of events whose interdistance R is less than r, the correlation integral is defined as follows:

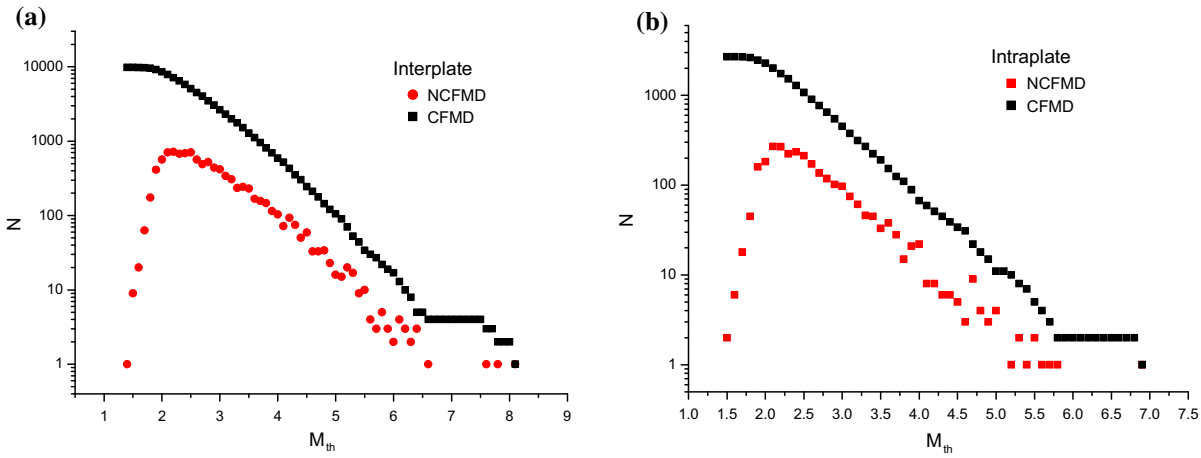

Figure 3
Non-cumulative and cumulative frequency-magnitude distribution of interplate (**a**) and intraplate (**b**) earthquake magnitude

Table 1

Number of events (N), completeness magnitude (Mc), number of events with magnitude larger or equal to the completeness magnitude (N) and b value calculated by the least square linear regression (LSR) and Aki-Utsu's formula (A–U)

Catalogue	N	M_c	N ($M \geq M_c$)	b value (LSR)	b value (A–U)
Intraplate	2696	2.2	2015	0.788 ± 0.016	0.715 ± 0.01
Interplate	9818	2.5	5780	0.718 ± 0.011	0.6012 ± 0.007

$$C(r) = \frac{2N_{R<r}}{N(N-1)}. \tag{13}$$

For fractal spatial point processes $C(r) \approx r^{d_f}$. The numerical value of the correlation dimension d_f is estimated as the slope of the line fitting the correlation integral versus r plotted in log–log scales in its approximately linear range by the least square method. Defining R_{max} as the maximum distance between two events of the dataset, the estimation of

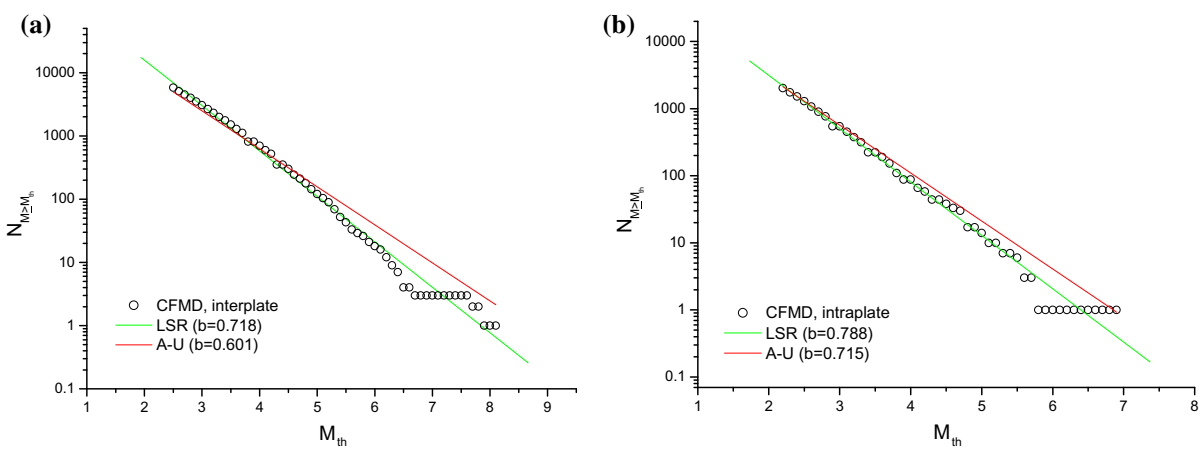

Figure 4
Comparison between the GR laws corresponding to the b value calculated by using the methods of A–U (red) and LSR (green) for the interplate (**a**) and intraplate (**b**) seismicity

the correlation dimension was performed between the 1% and the 30% (Dongsheng et al. 1994) of the R_{max}; these two limits would be sufficient to avoid finite-size effect visible at small and large spatial scales (Telesca et al. 2017a, b). We obtained the following values of the fractal dimension: 1.42 (interplate) and 1.53 (intraplate). We applied, then, the aftershock-depletion method based on NN (Zaliapin et al. 2008) with the found values of correlation dimension d_f and minimum magnitude that is the completeness magnitude. The third input parameter to the NN algorithm is the b value; since we obtained two different values of b for each seismic catalogue, we applied the NN algorithm varying the b value of the whole catalogue. Table 2 shows for each b-value of the whole catalogue, the number of background events and the b value calculated on the background seismicity by LSR and A–U methods, respectively.

After depleting the aftershocks the interplate seismicity contains from 2121 to 2168 events and the intraplate one contains from 1711 to 1716 events, depending on the input b value to the NN algorithm. Whatever is the value of input b, the obtained aftershock-depleted catalogues have almost the same size, confirming the robustness of the NN algorithm. For each aftershock-depleted catalogue we calculated the b value by using the two methods of LSR and A–U; both the aftershock-depleted catalogues have consistent b values whatever is the method used to calculate it. The b value of the background seismicity for the interplate seismicity remains still lower than that for the intraplate one, indicating that the interplate area is subjected to a larger stress than the intraplate zone.

Table 2

Number of background events after depleting the whole catalogue by NN algorithm with input b value calculated by using A–U and LSR methods

Input b value	Interplate seismicity	Intraplate seimicity
LSR	2121 (0.62_{LSR}; 0.74_{AU})	1716 (0.78_{LSR}; 0.71_{AU})
A–U	2168 (0.62_{LSR}; 0.73_{AU})	1711 (0.78_{LSR}; 0.70_{AU})

In brackets, the first value is the b calculated on the aftershock-depleted catalogue by using LSR method, while the second one is the b calculated on the aftershock-depleted catalogue by using the A–U method

Figure 5 shows the AF for both whole intraplate and interplate seismicity and the 95% confidence band in relationship with two types of surrogate sequences: 1000 Poissonian surrogates with the same rate as the original sequence (blue), and 1000 random surrogates obtained randomly shuffling the interevent times of the original sequence (red), conserving, thus, the interevent probability density function. For the interplate seismic sequence, we observe a crossover timescale at about $10^{4.4}$ s separating the Poissonian regime from the time-clusterized one, and a scaling region for timescales larger than the crossover with scaling exponent ~ 0.94, indicating a rather high time-clusterization of the events. The crossover roughly corresponds to the mean interevent time that for the interplate seismicity is about 6 h. Furthermore, the AF of the original sequence is well beyond the Poissonian 95% confidence band and the 95% confidence band based on 1000 random shuffles of the interevent times, indicating that it is significantly non Poissonian at intermediate and large timescales, and that its scaling behavior does not depend on the probability density function of the interevent times. The AF for the intraplate sequence is different from that of the interplate, since it is mostly embedded in both the 95% Poissonian and random shuffle confidence bands, indicating the absence of significant time-clusterization of the events.

The scaling behavior found for the interplate seismic sequence for timescales larger than the crossover is very likely due to the aftershock activation following the largest shock of magnitude 8.1.

Figure 6 shows the AF for the two catalogues depleted by using the NN algorithm with the two different b values as input.

The AF of the aftershock-depleted interplate sequences indicates clearly that the scaling behavior observed in the whole sequence is mostly affected by the aftershock activation. However, the clustering effect is still visible in the aftershock-depleted sequences at large timescales; this indicates that the background seismicity is characterized by some time-clusterization at large timescales, while the clustering phenomenon due to the aftershocks characterizes the time dynamics of the seismicity just at intermediate timescales. In fact, if the whole interplate sequence shows a crossover between Poissonian and time-

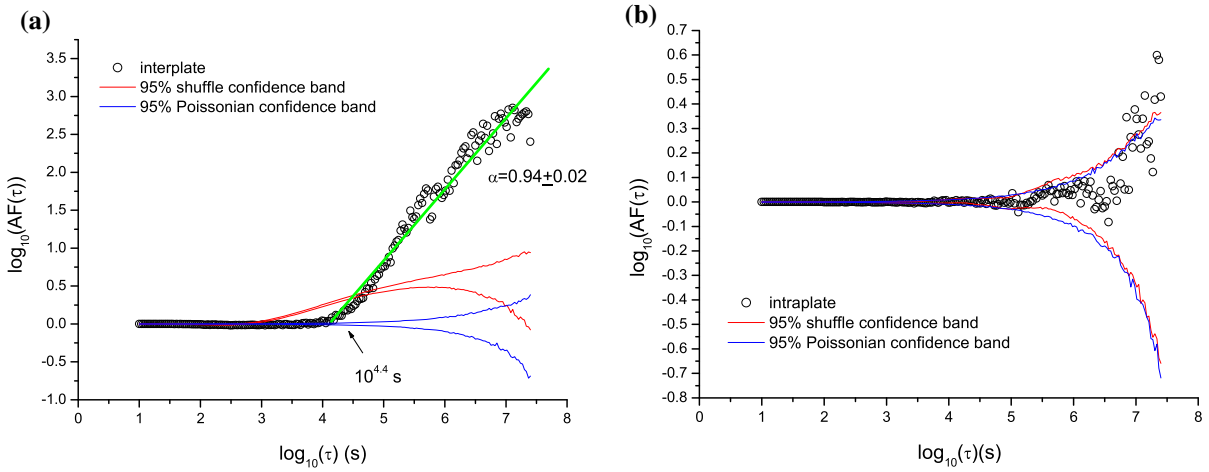

Figure 5
Allan Factor of the whole interplate (**a**) and intraplate (**b**) seismicity (black), and the 95% confidence band based on 1000 Poissonian surrogates (blue), and 1000 random surrogates obtained randomly shuffling the interevent times of the original sequence (red)

clusterization at about 7 h, the crossover in the AF of the aftershock-depleted ones shifts upward, indicating that the aftershocks characterize the time-clustering of the sequence at intermediate time scales. The AF of aftershock-depleted intraplate sequences (whatever is the input *b*-value to the NN algorithm) does not differ from the AF of the surrogates, and, similarly to the whole sequence, are not characterized by significant time-clusterization.

Figure 7 shows the fluctuation function F_n of the interevent times and magnitude series of both sequences plotted in log–log scales. The fluctuation function of the interplate interevent times (Fig. 7a) displays a two-fold scaling behavior with the scaling exponent at larger scales higher than that at lower scales; this two-fold behavior is very likely an effect of the mixture of background events and aftershocks that would be evidenced in the different ranges of their scaling. The 95% random shuffle confidence interval based on 1000 random shuffles of the original interevent series is [0.466, 0.541] that indicates that the obtained scaling exponents are significantly different from random surrogates. The scaling exponent of the magnitudes of interplate sequence is $\sim$ 0.755 [0.470, 0.543], which indicates that this series is significantly persistent. For the intraplate seismicity we obtained $\sim$ 0.582 [0.456, 0.555] and $\sim$ 0.524 [0.453, 0.558] for the interevent times and magnitudes respectively. Considering the confidence intervals, the scaling is significantly different from the random for the interevent times and magnitudes of the interplate sequence indicating a persistent dynamics, while for the intraplate both the interevent times and magnitudes are not significantly distinguishable from random. We applied the DFA also to the interevent times and magnitudes of the aftershock-depleted sequences and the scaling exponents are shown in Tables 3 and 4. The DFA curve of interplate interevent times of the aftershock-depleted seismicity is similar to that of the whole seismicity (Fig. 8); in fact, two scaling regions are clearly identified with the scaling exponent at larger scales higher than that at smaller scales. However the scaling exponent at smaller scales is about 0.5, indicating the absence of correlation structures at these scales; this is consistent with the results obtained by applying the AF analysis and indicates that the aftershock-depletion has removed the correlations at small scales, while keeping those at large scales. The fluctuation functions of all the other series (interplate magnitudes and intraplate interevent times and magnitudes) of the aftershock-depleted seismicity (not shown) are characterized by purely random behavior without any significant evidence of persistence.

We applied the HVG to the interevent and magnitude series of the two seismic sequences,

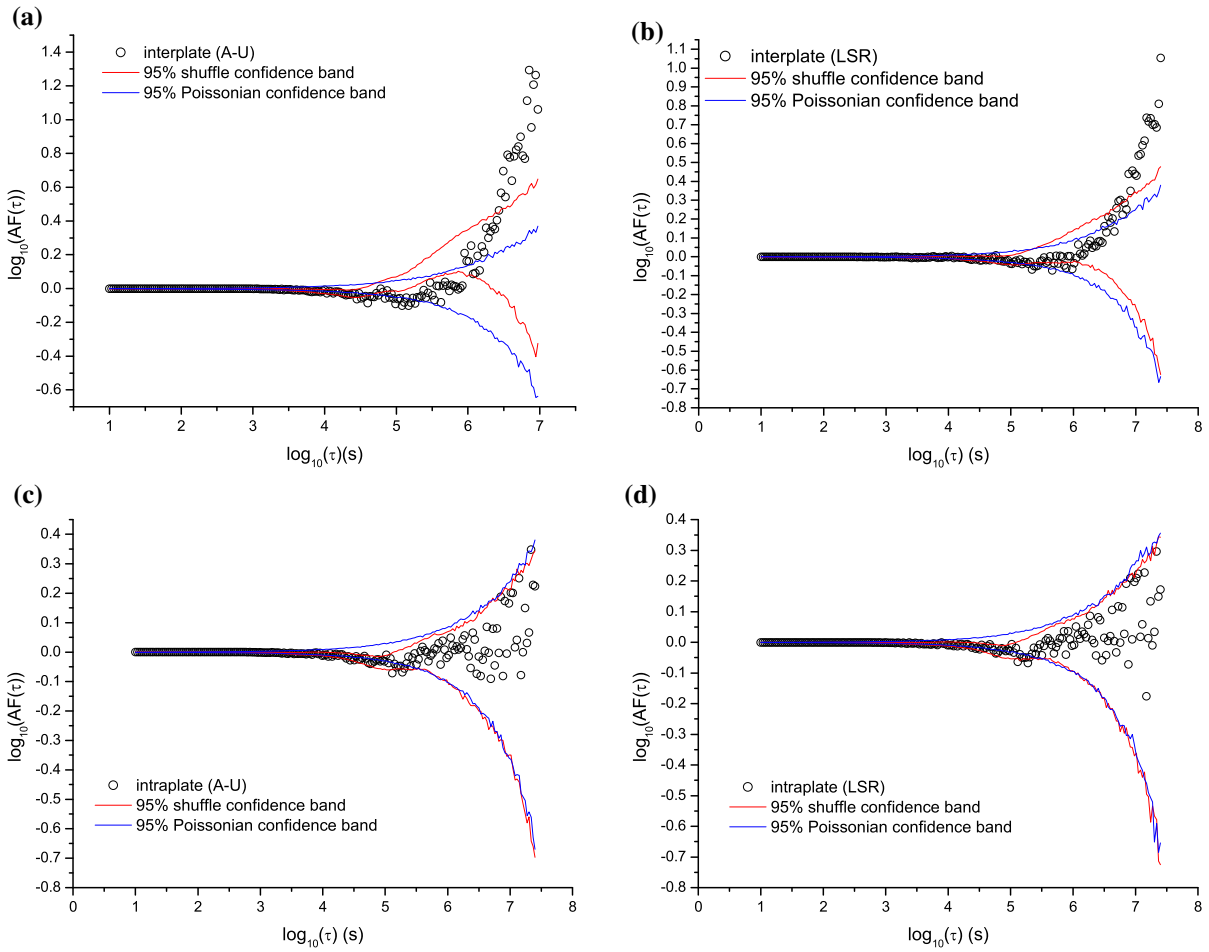

Figure 6

Allan Factor of the catalogues depleted by the NN algorithm using the input *b*-value calculated by means of the A–U (**a**, **c**) and LSR (**b**, **d**) methods for the interplate (a, b) and intraplate (**c**, **d**) seismicity along with the 95% confidence band based on 1000 Poissonian surrogates (blue), and 1000 random surrogates obtained randomly shuffling the interevent times of the original sequence (red)

investigating the time-reversibility/irreversibility by using the Kullback–Leibler divergence (KLD) to quantify the separation between the in-going and out-going degree distributions. Figure 9 shows, as an example the time series of in-going connectivity degree k_{in} and the that of the out-going connectivity degree k_{out} for the magnitude series of the intraplate sequence.

We also calculated the KLD for 1000 shuffles and compared the mean value and standard deviation of the shuffles with the KLD of the original series (Telesca et al. 2018). Considering practically time-reversible those series whose KLD is within the 1 standard deviation range of the KLD calculated for the shuffles, the magnitude series and the interevent times of the interplate seismicity appear time-irreversible, along with the interevent times of the intraplate catalogue (Fig. 10a). The magnitudes of the intraplate catalogue (Fig. 10a) and both magnitudes and interevent times of all the aftershock-depleted catalogues are characterized by time-reversibility (Fig. 10b, c); this seems to be consistent with the recent concept of "topological isotropy" introduced by Telesca et al. (2020), who analysed the topological properties of the Italian and Taiwanese seismicity by the VG method, and found that the aftershocks would induce a sort of anisotropy in the topological representation of the time distribution of the earthquakes.

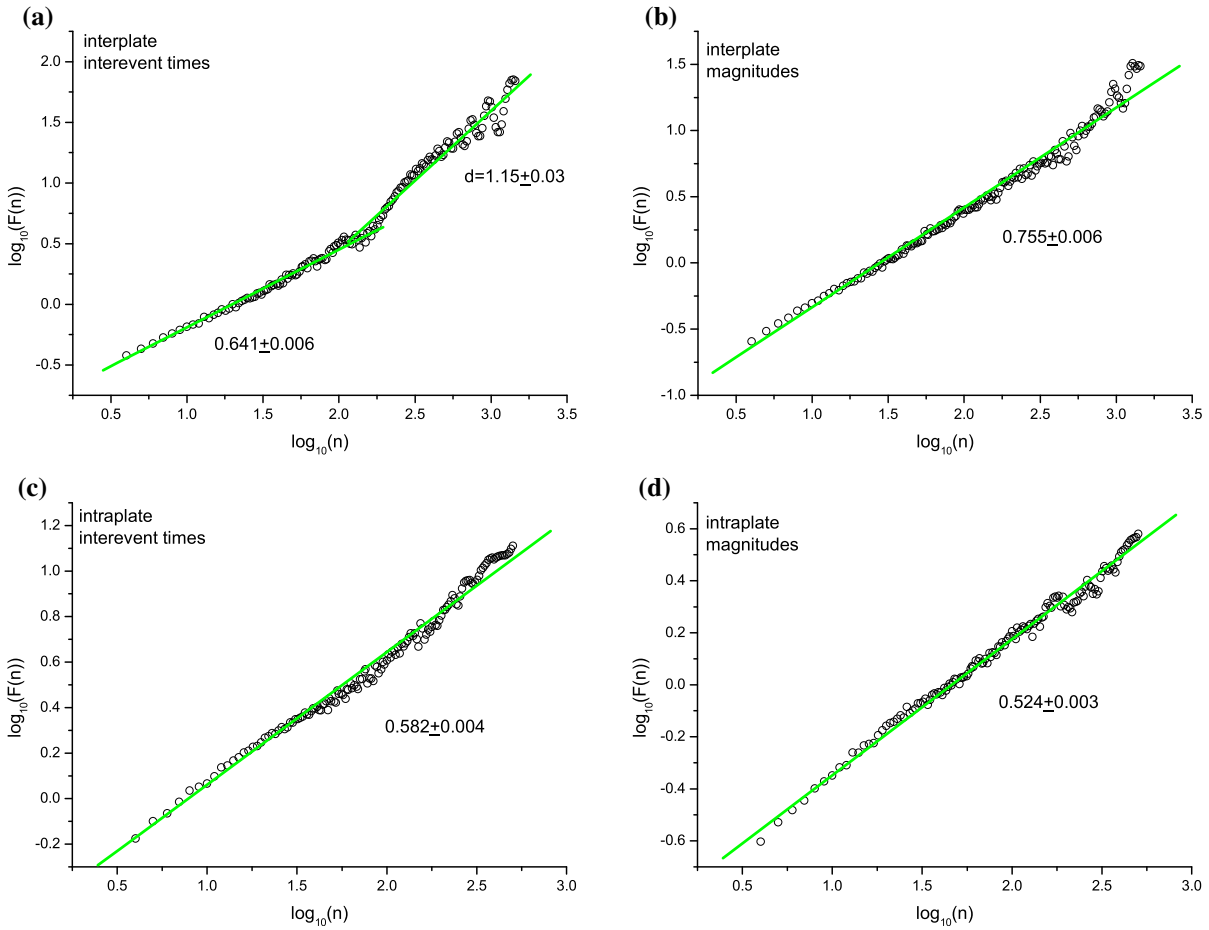

Figure 7
Fluctuation function F_n of the interevent times (**a**, **c**) and magnitude (**b**, **d**) series of interplate and intraplate seismicity plotted in log–log scales

Table 3

DFA exponent for interevent times of background seismicity after depleting the whole catalogue by NN algorithm with input b value calculated by using A–U and LSR methods

Input *b* value	Interplate seimicity	Intraplate seimicity
A–U	[0.455, 0.554]	0.554 [0.454, 0.559]
LSR	[0.463, 0.555]	0.554 [0.456, 0.558]

In brackets, the 95% shuffle confidence band. For the interplate aftershock depleted sequences only the 95% shuffle confidence band is reported

Table 4

DFA exponent for magnitude series of background seismciity after depleting the whole catalogue by NN algorithm with input b value calculated by using A–U and LSR methods

Input *b* value	Interplate seimicity	Intraplate seimicity
A–U	0.503 [0.458, 0.558]	0.505[0.455, 0.560]
LSR	0.525 [0.454, 0.558]	0.505 [0.457, 0.562]

In brackets, the 95% shuffle confidence band

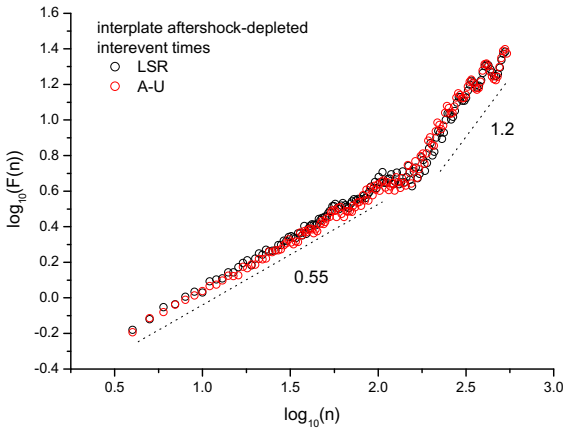

Figure 8
Fluctuation function F_n of the interevent times of interplate aftershock-depleted seismicity plotted in log–log scales

5. Discussion

We investigated the time dynamics of the 2007–2014 intraplate and interplate seismicity in the area where the large Iquique earthquake occurred in 2014 in the far north of Chile.

The the different b values (b = 0.72–0.79 for the intraplate catalogue and b = 0.60–0.72 for the interplate catalogue) agree with previous studies performed on subduction zones and continental crust (Scholz 2015). Métois et al. (2016) shows a lower coupling of the Iquique zone, which confirms the low b-value that we obtained for the interplate zone, indicating a stress state different from that of the intraplate zone.

The role of aftershocks, especially for the interplate seismicity, has been evidenced by using two different statistical tools, namely the AF and the DFA, both aiming at identifying scaling structures in time series. The AF not only has discriminated between Poissonian (or uncorrelated) behavior and time-clusterized (or correlated) behavior, but it has also furnished information on the time scales that are involved in the clustering phenomenon shown by the seismic sequence and on the intensity of such clustering quantified by the scaling exponent α. At a certain time scale the AF provides a quantitative measure of the variability exhibited by the earthquake rate (Lowen et al. 1997). In case of interplate seismicity, the event rate variability is power-law-shaped as indicated by the power-law behavior of the AF for time scales larger than the crossover, which is about 7 h; this crossover represents the minimum time scale that makes possible to discern clustering behavior; thus for time scales lower than the crossover the seismic sequence behaves as a Poisson process, where the events are uncorrelated and independent among each other. Identifying time-clustering in the interplate sequence indicates that the seismic process is not random or uncorrelated but governed by

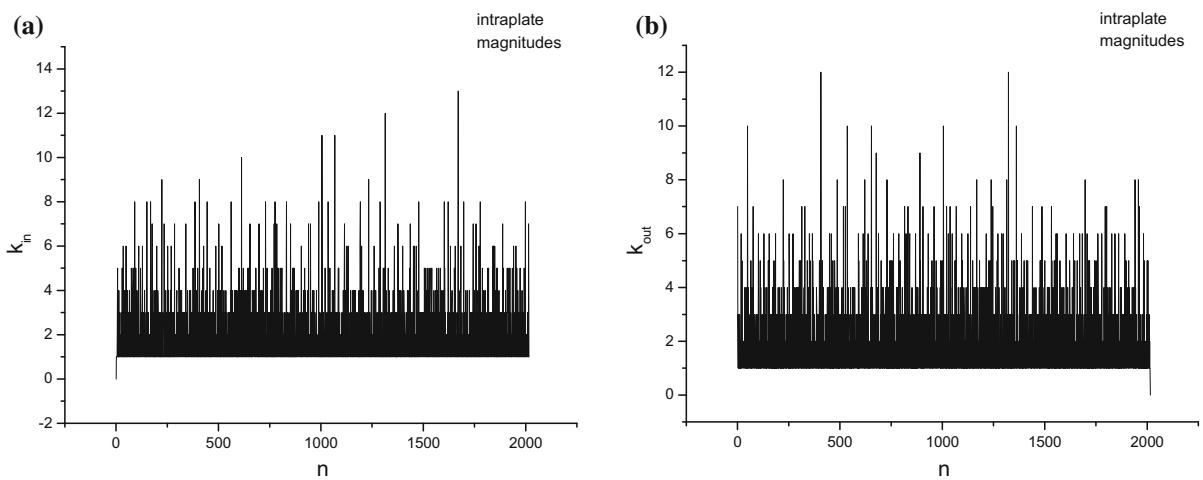

Figure 9
Time series of in-going connectivity degree k_{in} (**a**) and out-going connectivity degree k_{out} (**b**) for the magnitude series of the intraplate sequence

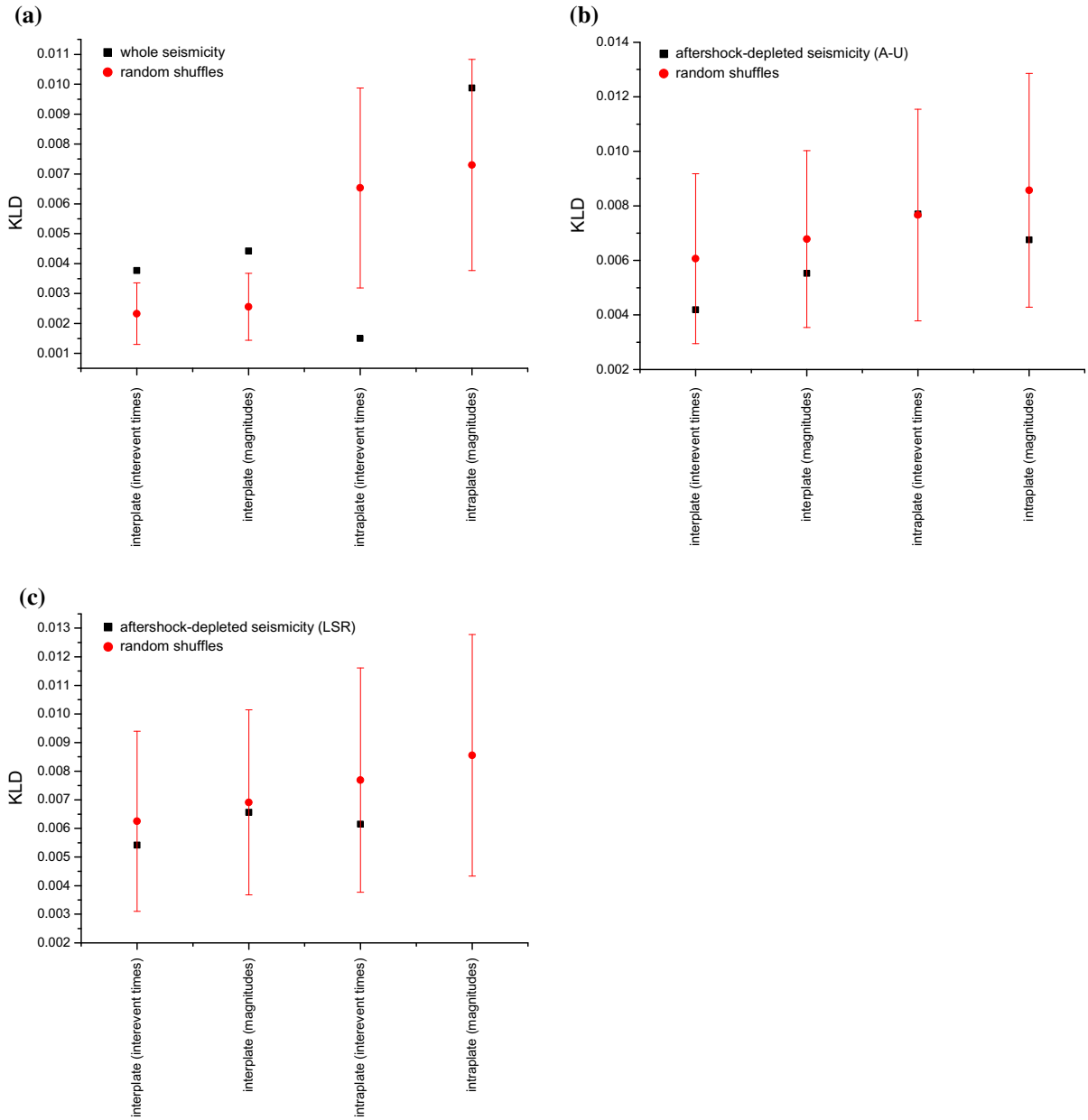

Figure 10
KLD for the interevent and magnitude series for both the whole catalogues (**a**) and aftershock-depleted ones by using the input *b*-value calculated by the A–U (**b**) and LSR (**c**) method

memory phenomena that link each event to the others. This picture is in agreement with Sippl et al. (2019) who observed that interplate events "are more episodic in their occurrence, with sharp rate changes that correspond to major aftershock series (2007 M 7.7 Tocopilla and 2014 M 8.1 Iquique earthquakes), and a rather low background rate in-between these". Such "episodicity" mirrors the clustering character identified by the AF analysis, which suggests that the interplate event rate does change through time with sharp increases interspersed with low seismic activity. Contrarily to interplate seismicity, the intraplate

one does not show significant time-clustering; this also agrees with Sippl et al. (2019) who found that the intraplate seismicity "shows a rather stable background activity". From a physical perspective, the clustering found in the interplate seismicity and revealed by the AF is due to the aftershocks that are triggered by large events. In fact, after removing the aftershocks the interplate sequence loses its clustering behavior at intermediate time scales, and the crossover shifts upward. The power-law behavior of the AF might be put in relationship with the band limited power law (LPL) model that describes the temporal decay of the increased local rate of seismicity after large earthquakes (Davidsen et al. 2015); however, more investigation is necessary to establish possible direct relationship between the parameters of the AF and those of LPL model for aftershocks.

The analysis of long-range correlations in the magnitude time series has been subject of investigation in several studies, since magnitude represent one of the crucial parameter in the framework of seismic hazard assessment. Telesca et al. (2016) found that the scaling exponent of the magnitude time series calculated by the DFA increased during the 2011–2014 reactivation of the volcanic activity at El Hierro, Canary Islands (Spain). Varotsos et al. (2014) used the DFA of the magnitude series in several seismic region highlighting the relationship between the variation of the scaling exponent and strong incoming earthquakes. Lennartz et al. (2008) investigated the long-range correlations of the magnitude series of Northern and Southern California seismicity by using the DFA to reveal that earthquake magnitude are characterized by long-term memory. Varotsos et al. (2012) found that the magnitudes of California seismicity change their status from uncorrelated to correlated before the occurrence of large shocks. Telesca et al. (2017a, b) found that the magnitude series of the reservoir-induced seismicity of Aswan (Egypt) are persistently correlated indicating that if magnitude tends to increase or decrease in a certain period, very likely it will keep on increasing or decreasing in the next period.

The persistent character of the magnitudes of interplate seismicity suggests that they are not independent, indicating that if the magnitude increase (or decrease) in a certain period, it will likely increase (or decrease) in the next period. Such correlation structure in the magnitudes of the interplate seismicity disappears after removing the aftershocks that could be considered as the main source of persistence in the magnitude series. Contrarily to magnitudes, the interevent times of interplate seismicity keeps still persistent character at large scales after removing the aftershocks, and this is agreement with the AF results for the same series. The aftershocks are also responsible of this behavior because their effect on the interevent times at intermediate scales is annihilated. The whole and aftershock-depleted intraplate seismicity show random behavior in both the magnitudes and interevent times; this indicates that earthquakes are not correlated in time as well as in magnitude domain. The aftershocks represent only 15% of the whole intraplate seismicity, while they represent about 60% of the whole interplate seismicity; thus their effect is much less intense in the intraplate seismicity than in the interplate one, and their removal does not change significantly the correlation properties of the intraplate earthquakes in time and magnitude.

The topological results obtained by applying the visibility graph seem consistent with the fractal results. The time-reversibility/irreversibility has become important in characterizing natural phenomena and observed time series (Daw et al. 2000). Time-reversibility (time-irreversibility) indicates that statistical properties do not depend (depend) on whether one observes the behavior of a system as time proceeds in its natural or reverse direction. Time-irreversibility implies that the system is characterized by nonlinear dynamics, non-Gaussian noise, or both (Stone et al. 1996). Thus, significant time-irreversibility excludes Gaussian linear processes or static nonlinear transformations of such processes as possible models for the generating dynamics of a system (Daw et al. 2000). The time-irreversibility characterizing the interplate seismicity is a clear sign of the nonlinearity of the seismic process that is constituted in the majority by aftershocks. Aftershocks are responsible not only of the time-clustering behavior of the interplate seismicity, but also of its nonlinearity, typical of system driven out-of-equilibrium (Roldan and Parrondo 2010). The aftershock removal makes all the catalogues time-reversible

both in the magnitudes and interevent times; this could be explained by a reduction of the nonlinearity of the seismic process. The presence of aftershocks "favors a time direction" in the evolution of the seismic process, because they are produced after the occurrence of a large shock. The dynamical properties of the background seismicity, which remains after removing the aftershocks, are substantially independent upon the time direction of observation. This agrees with the concept of "topological isotropy" that was stated by Telesca et al. (2020) when comparing the forward and backward visibility graphs of seismicity of Italy and Taiwan with and without aftershocks.

6. Conclusions

Our main findings can be summarized as follows:

(i) the different b values (b = 0.72–0.79 for the intraplate catalogue and b = 0.60–0.72 for the interplate catalogue) agree with previous studies performed on subduction zones and continental crust (Scholz 2015). Métois et al. (2013) shows a lower coupling of the Iquique zone, which confirms the low b value that we obtained for the interplate zone, indicating a stress state different from that of the intraplate zone;

(ii) the interplate seismicity is characterized by significant time-clustering especially at large time scales, while the intraplate catalogue does not show significant clustering phenomenon. After removing the aftershocks, the interplate catalogue still keeps its clustering phenomenon but at higher timescales, thus shortening its clustering time scale range. The intraplate catalogue remains Poissonian for most of the time scale. This result suggests that aftershocks play an important role in characterizing the time distribution of the seismicity in the interplate zone, whose background seismicity is, nevertheless, still characterized by a certain clustering behavior;

(iii) persistent fluctuations characterize the interevent times and the magnitudes of the interplate catalogue, while uncorrelated fluctuations characterize the behavior of interevent intervals and magnitudes of the whole as well as aftershock-depleted intraplate catalogue. The interevent time series of the aftershock-depleted interplate catalogue are still characterized by non random behavior at large scales; and this is in accordance with the results obtained by the Allan Factor; the magnitudes, instead, are featured by uncorrelated behavior;

(iv) the magnitudes and the interevent times of the interplate seismicity and the interevent times of the intraplate seismicity appear time-irreversible; while the magnitudes of the intraplate seismicity and both magnitudes and interevent times of all the aftershock-depleted catalogues are characterized by time-reversibility;

(v) it is evidenced a different role played by the aftershocks in the intraplate and interplate zones, that needs to be further explored.

Acknowledgements

DP thanks Proyecto Fondecyt N°11160452. VM thanks Proyecto Fondecyt N°1161711. The authors are grateful to I. Zaliapin for providing the code for nearest-neighbour analysis.

References

Aki, K. (1965). Maximum likelihood estimate of b in the formula log(N) = a-bM and its confidence limits. *Bulletin Earthquake Research Institute Tokyo University, 43,* 237–239.

Andrieux, D., Gaspard, P., Ciliberto, S., Garnier, N., Joubaud, S., & Petrosyan, A. (2007). Entropy production and time asymmetry in nonequilibrium fluctuations. *Physical Review Letters, 98,* 150601.

Baiesi, M., & Paczuski, M. (2004). Scale-free networks of earthquakes and aftershocks. *Physics Review E., 69,* 066106.

Cammarota, C., & Rogora, E. (2007). Time reversal, symbolic series and irreversibility of human heartbeat. *Chaos, Solitons and Fractals, 32,* 1649–1654. https://doi.org/10.1016/j.chaos.2006.03.126.

Comte, D., & Pardo, M. (1991). Reappraisal of Great Historical Earthquakes in the Northern Chile and Southern Peru Seismic Gaps. *Natural Hazards, 4,* 23–44.

Costa, M. D., Peng, C.-K., & Goldberger, A. L. (2008). Multiscale analysis of heart rate dynamics: Entropy and time irreversibility measures. *Cardiovascular Engineering, 8,* 88–93.

Cover, T. M., & Thomas, J. A. (2006). *Elements of information theory*. New Jersey: Wiley.

Davidsen, J., Gu, C., & Baiesi, M. (2015). Generalized Omori-Utsu law for aftershock sequences in southern California. *Geophysics Journal of International, 201,* 965–978.

Daw, C. S., Finney, C. E. A., & Kennel, M. B. (2000). Symbolic approach for measuring temporal ''irreversibility''. *Physical Review E, 62,* 1912–1921.

Derode, B., & Campos, J. (2019). Energy budget of intermediate-depth earthquakes in northern Chile: Comparison with shallow earthquakes and implications of rupture velocity models used. *Geophysical Research Letters, 46,* 2484–2493.

Diks, C., van Houwelingen, J. C., Takens, F., & DeGoede, J. (1995). Reversibility as a criterion for discriminating time series. *Physics Letters A, 201,* 221–228.

Dongsheng, L., Zhaobi, Z., & Binghong, W. (1994). Research into the multifractal of earthquake spatial distribution. *Tectonophysics, 233,* 91–97.

Doxas, I., Dennis, S., & William, L. O. (2010). The dimensionality of discourse. *Proceedings of National Academy of Science, 107,* 4866–4871.

Gaspard, P. (2004). Time-reversed dynamical entropy and irreversibility in Markovian random processes. *Journal of Statistical Physics, 117,* 599–615.

Goebel, T. H. W., Schorlemmer, D., Becker, T. W., Dresen, G., & Sammis, C. G. (2013). Acoustic emissions document stress changes over many seismic cycles in stick-slip experiments. *Geophysical Research Letters, 40,* 2049–2054.

Grassberger, P., & Procaccia, I. (1983). Measuring the strangeness of strange attractors. *Physica D: Nonlinear Phenomena, 9,* 189–208.

Gutenberg, R., & Richter, C. F. (1944). Frequency of earthquakes in California. *Bulletin of the Seismological Society of America, 34,* 185–188.

Han, Q., Wang, L., Xu, J., Carpinteri, A., & Lacidogna, G. (2015). A robust method to estimate the b-value of the magnitude–frequency distribution of earthquakes. *Chaos Solitons and Fractals, 81,* 103–110.

Hayes, G. P., Herman, M. W., Barnhart, W. D., Furlong, K. P., Riquelme, S., Benz, H. M., et al. (2014). Continuing megathrust earthquake potential in Chile after the 2014 Iquique earthquake. *Nature, 512,* 295–298.

Ishimoto, M., & Iida, K. (1939). Observations of earthquakes registered with the microseismograph constructed recently. *Bulletin Earthquake Research Institute, University of Tokyo, 17,* 443–478.

Kárník, V., & Klíma, K. (1993). Magnitude-frequency distribution in the European-Mediterranean earthquake regions. *Tectonophysics, 220,* 309–323.

Kausel, E. (1986). Los terremotos de Agosto de 1868 y Mayo de 1877 que afectaron el sur del Perú norte de Chile. *Boletín de la Academia Chilena de Ciencias, 3,* 8–12.

Kawai, R., Parrondo, J. M. R., & Van den Broeck, C. (2007). Dissipation: The phase-space perspective. *Physical Review Letters, 98,* 080602. https://doi.org/10.1103/PhysRevLett.98.080602.

Lacasa, L., Luque, B., Ballesteros, F., Luque, J., & Nuno, J. C. (2008). From time series to complex networks: The visibility graph. *Proceedings of the National academy of Sciences of the United States of America, 105,* 4972–4975. https://doi.org/10.1073/pnas.0709247105.

Lacasa, L., Luque, B., Luque, J., & Nuño, J. C. (2009). The visibility graph: A new method for estimating the Hurst exponent of fractional Brownian motion. *EPL (Europhysics Letters), 86*(3), 30001.

Lacasa, L., Nuñez, A., Roldán, E., Parrondo, J. M. R., & Luque, B. (2012). Time series irreversibility: A visibility graph approach. *European Physical Journal B: Condensed Matter and Complex Systems, 85,* 217. https://doi.org/10.1140/epjb/e2012-20809-8.

Lennartz, S., Livina, V. N., Bunde, A., & Havlin, S. (2008). Long-term memory in earthquakes and the distribution of interoccurrence times. *Europhysics Letters, 81,* 69001.

Lomnitz, C. (2004). Major earthquakes of Chile: A historical survey, 1535–1960. *Seismological Research Letters, 75,* N3.

Lowen, S. B., Cash, S. S., Poo, M.-M., & Teich, M. C. (1997). Quantal neurotransmitter secretion rate exhibits fractal behavior. *The Journal of Neuroscience, 17,* 5666–5677.

Luque, B., Lacasa, L., Luque, J., & Ballesteros, F. (2009). Horizontal visibility graphs: Exact results for random time series. *Physical Review E, 80,* 046103.

Malgrange, M., & Madariaga, R. (1983). Complex distribution of large thrust and normal fault earthquakes in the Chilean subduction zone. *Geophysical Journal International, 73*(2), 489–505.

Métois, M., Socquet, A., & Vigny, C. (2012). Interseismic coupling, segmentation and mechanical behavior of the central Chile subduction zone. *Journal of Geophysics Research, 117,* B03406.

Métois, M., Vigny, C., & Socquet, A. (2016). Interseismic coupling, megathrust earthquakes and seismic swarms along the Chilean subduction zone (38°–18°S). *Pure and Applied Geophysics, 173,* 1431–1449.

Montessus de Ballore, F., (1911–1916). Historia Sísmica de los Andes Meridionales, al sur del Paralelo XVI, Cervantes, Santiago de Chile.

Naylor, M., Greenhough, J., McCloskey, J., Bell, A. F., & Main, I. G. (2009). Statistical evaluation of characteristic earthquakes in the frequency magnitude distributions of Sumatra and other subduction zone regions. *Geophysical Research Letters, 36,* L20303. https://doi.org/10.1029/2009GL040460.

Parrondo, J. M. R., Van den Broeck, C., & Kawai, R. (2009). Entropy production and the arrow of time. *New Journal of Physics, 11,* 073008.

Peng, C.-K., Havlin, S., Stanley, H. E., & Goldberger, A. L. (1995). Quantification of scaling exponents and crossover phenomena in nonstationary heartbeat time series. *CHAOS, 5,* 82–87.

Peresan, A., & Gentili, S. (2020). Identification and characterisation of earthquake clusters: A comparative analysis for selected sequences in Italy and adjacent regions. *Bollettino di Geofisica Teorica ed Applicata, 61,* 57–80.

Peyrat, S., Madariaga, R., Buforn, E., Campos, J., Asch, G., & Vilotte, J. P. (2010). Kinematic rupture process of the 2007 Tocopilla earthquake and its main aftershocks from teleseismic and strongmotion data. *Geophysics Journal International, 182*(3), 1411–1430.

Roldan, E., & Parrondo, J. M. R. (2010). Estimating dissipation from single stationary trajectories. *Physical Review Letters, 105,* 150607.

Ruegg, J. C., Campos, J., Armijo, R., Barrientos, S., Briole, P., Thiele, R., et al. (1996). The Mw = 8.1 Antofagasta (North Chile) earthquake of July 30, 1995: First results from teleseismic and geodetic data. *Geophysics Research Letters, 23*(9), 917–920.

Ruiz, S., & Madariaga, R. (2018). Historical and recent large megathrust earthquakes in Chile. *Tectonophysics*, *733*, 37–56.

Schleussner, C.-F., Divine, D. V., Donges, J. F., Miettinen, A., & Donner, R. V. (2015). Indications for a North Atlantic ocean circulation regime shift at the onset of the Little Ice Age. *Climate Dynamics, 45,* 3623–3633. https://doi.org/10.1007/s00382-015-2561-x.

Scholz, C. H. (1968). Microfracturing and the inelastic deformation of rock in compression. *Journal of Geophysical Research, 73,* 1417–1432.

Scholz, C. H. (2015). On the stress dependence of the earthquake b value. *Geophysical Research Letters, 42,* 1399–1402.

Schorlemmer, D., Wiemer, S., & Wyss, M. (2005). Variations in earthquake-size distribution across different stress regimes. *Nature, 437,* 539–542.

Shi, Y., & Bolt, B. A. (1982). The standard error of the magnitude-frequency b-value. *Bulletin of the Seismological Society of America, 72,* 1677–1687.

Sippl, C., Schurr, B., Asch, G., & Kummerow, J. (2018a). Seismicity structure of the northern Chile forearc from > 100,000 double-difference relocated hypocenters. *Journal of Geophysical Research Solid Earth Solid Earth, 123,* 4063–4087.

Sippl, C., Schurr, B., Asch, G., & Kummerow, J. (2018b). Catalogue of earthquake hypocenters for northern Chile compiled from IPOC (plus auxiliary) seismic stations. *GFZ Data Services*. https://doi.org/10.5880/GFZ.4.1.2018.001.

Sippl, C., Schurr, B., John, T., & Hainzl, S. (2019). Filling the gap in a double seismic zone: Intraslab seismicity in Northern Chile. *Lithos, 346–347,* 105155.

Spada, M., Tormann, T., Wiemer, S., & Enescu, B. (2013). Generic dependence of the frequency-size distribution of earthquakes on depth and its relation to the strength profile of the crust. *Geophysical Research Letters, 40,* 709–714.

Stone, L., Landan, G., & May, R. M. (1996). Detecting time's arrow: A method for identifying nonlinearity and deterministic chaos in time-series data. *Proceeding of Royal Society of London Series B, 263,* 1509–1513.

Telesca, L., & Chen, C.-C. (2019). Fractal and spectral investigation of the shallow seismicity in Taiwan. *Journal of Asian Earth Sciences*. https://doi.org/10.1016/j.jseaes.2018.10.009.

Telesca, L., Chen, C.-C., & Lovallo, M. (2020). Investigating the relationship between seismological and topological properties of seismicity in Italy and Taiwan. *Pure and Applied Geophysics*. https://doi.org/10.1007/s00024-020-02470-8.

Telesca, L., Cuomo, V., Lapenna, V., & Macchiato, M. (2001). Statistical analysis of fractal properties of point processes modelling seismic sequences. *Physics Earth Planetary International, 125,* 65–83.

Telesca, L., Cuomo, V., Lapenna, V., & Vallianatos, F. (2000). Self-similarity properties of seismicity in the Southern Aegean area. *Tectonophysics, 321,* 179–188.

Telesca, L., Fat-Elbary, R., Stabile, T. A., Haggag, M., & Elgabry, M. (2017a). Dynamical characterization of the 1982–2015 seismicity of Aswan region (Egypt). *Tectonophysics, 712–713,* 132–144.

Telesca, L., Flores-Márquez, E. L., & Ramírez-Rojas, A. (2018). Time-reversibility in seismic sequences: Application to the seismicity of Mexican subduction zone. *Physica A: Statistical Mechanics and its Applications*, *492*, 1373–1381.

Telesca, L., Kadirov, F., Yetirmishli, G., Safarov, R., Babayev, G., & Ismaylova, S. (2017b). Statistical analysis of the 2003–2016 seismicity of Azerbaijan and surrounding areas. *Journal of Seismology, 21,* 1467–1485.

Telesca, L., & Lovallo, M. (2008). Analysis of the temporal properties in car accident time series. *Physica A, 387,* 3299–3304.

Telesca, L., & Lovallo, M. (2009). Non-uniform scaling features in Central Italy seismicity: A non-linear approach in investigating seismic patterns and detection of possible earthquake precursors. *Geophysical Research Letters, 36,* L01308.

Telesca, L., & Lovallo, M. (2010). Long-range dependence in tree-ring width time series of Austrocedrus chilensis revealed by means of the detrended fluctuation analysis. *Physica A, 389,* 4096–4104.

Telesca, L., & Lovallo, M. (2011). Analysis of time dynamics in wind records by means of multifractal detrended fluctuation analysis and Fisher-Shannon information plane. *Journal of Statics Mechanics, 201,* P07001.

Telesca, L., Lovallo, M., Lopez, M. C., & Molist, J. M. (2016). Multiparametric statistical investigation of seismicity occurred at El Hierro (Canary Islands) from 2011 to 2014. *Tectonophysics, 672–673,* 121–128. https://doi.org/10.1016/j.tecto.2016.01.045.

Telesca, L., Mohamed, A. E.-E. A., ElGabry, M., El-hady, S., & Abou Elenean, K. M. (2012). Time dynamics in the point process modelling of seismicity of Aswan area (Egypt). *Chaos, Solitons and Fractals, 45,* 47–55.

Thurner, S., Lowen, S. B., Feurstein, M. C., Heneghan, C., Feichtinger, H. G., & Teich, M. C. (1997). Analysis, synthesis, and estimation of fractal-rate stochastic point processes. *Fractals, 5,* 565–595.

Tormann, T., Enescu, B., Woessner, J., & Wiemer, S. (2015). Randomness of megathrust earthquakes implied by rapid stress recovery after the Japan earthquake. *Nature Geoscience, 8,* 152–158.

Utsu, T. (1999). Representation and analysis of the earthquake size distribution: A historical review and some new approaches. *Pageoph, 155,* 509–535.

Varotsos, P., Sarlis, N., & Skordas, E. (2012). Scale-specific order parameter fluctuations of seismicity before mainshocks: Natural time and detrended fluctuation analysis. *Europhysics Letters, 99*(59), 001.

Varotsos, P. A., Sarlis, N. V., & Skordas, E. S. (2014). Study of the temporal correlations in the magnitude time series before major earthquakes in Japan. *Journal of Geophysics Research Space Physics, 119,* 9192–9206.

Vidal Gormaz, F., (1877). Hundimiento o solevantamiento de los archipiélagos australes de Chile. Santiago, Imprenta Mejía, p. 1901.

Wang, Q., Kulkarni, S. R., & Verdú, S. (2005). Divergence estimation of continuous distributions based on data-dependent partitions. *IEEE Transactions on Information Theory, 51,* 3064–3074.

Weiss, G. (1975). Time-reversibility of linear stochastic processes. *Journal of Applied Probability, 12,* 831–836.

Wiemer, S. (2001). A software package to analyze seismicity: ZMAP, 2001. *Seismological Research Letters, 72,* 373–382.

Wiemer, S., & Wyss, M. (2000). Minimum magnitude of complete reporting in earthquake catalogs: Examples from Alaska, the western United States, and Japan. *Bulletin of the Seismological Society of America, 90,* 859–869.

Woessner, J., & Wiemer, S. (2005). Assessing the quality of earthquake catalogues: Estimating the magnitude of completeness and its uncertainty. *Bulletin of the Seismological Society of America, 95,* 684–698.

Wyss, M. (1973). Towards a physical understanding of the earthquake frequency distribution. *Geophysics Journal of Research Astronomy Society, 31,* 341–359.

Yang, A. C., Hseu, S. S., Yien, H. W., Goldberger, A. L., & Peng, C.-K. (2003). Linguistic analysis of the human heartbeat using frequency and rank order statistics. *Physical Review Letters, 90,* 108–109. https://doi.org/10.1103/PhysRevLett.90.108103.

Zaliapin, I., & Ben-Zion, Y. (2013). Earthquake clusters in southern California, I: Identification and stability. *Journal of Geophysical Research, 118,* 2847–2864. https://doi.org/10.1002/jgrb.50179.

Zaliapin, I., & Ben-Zion, Y. (2016). Discriminating characteristics of tectonic and human-induced seismicity. *Bulletin of the Seismological Society of America*. https://doi.org/10.1785/0120150211.

Zaliapin, I., Gabrielov, A., Wong, H., & Keilis-Borok, V. I. (2008). Clustering analysis of seismicity and aftershock identification. *Physical Review Letters, 101,* 018501.

(Received September 13, 2019, revised June 26, 2020, accepted July 15, 2020)